A generic seismic risk protocol for energy production sites

Grigoratos, Iason; Schultz, Ryan; van Ginkel, Janneke; Gunatilake, Thanushika; Wiemer, Stefan; van der Wal, Jorien L.N.; Muntendam-Bos, Annemarie G.

DOI
10.1007/s10518-024-02088-4

Publication date
2025

Document Version
Final published version

Published in
Bulletin of Earthquake Engineering

Citation (APA)
Grigoratos, I., Schultz, R., van Ginkel, J., Gunatilake, T., Wiemer, S., van der Wal, J. L. N., & Muntendam-Bos, A. G. (2025). A generic seismic risk protocol for energy production sites. *Bulletin of Earthquake Engineering*, *23*(4), 1325-1347. https://doi.org/10.1007/s10518-024-02088-4

Bulletin of Earthquake Engineering (2025) 23:1325–1347
https://doi.org/10.1007/s10518-024-02088-4

ORIGINAL ARTICLE

A generic seismic risk protocol for energy production sites

Iason Grigoratos[1] · Ryan Schultz[1] · Janneke van Ginkel[1] · Thanushika Gunatilake[1] · Stefan Wiemer[1] · Jorien L.N. van der Wal[2] · Annemarie G. Muntendam-Bos[2,3]

Received: 21 June 2024 / Accepted: 7 December 2024 / Published online: 13 February 2025

Abstract
Activities related to energy production have been linked with felt (and in some cases damaging) earthquakes. Notable examples include hydraulic fracturing, wastewater disposal, geothermal systems, coal mining, carbon storage and hydropower dams. As the demand for energy continues to grow, new frontiers in energy exploration will emerge - some with the potential for induced seismicity. Thus, there is a clear need for a source-agnostic seismic risk protocol that can be applied to any activity or region. This study outlines one such implementation that uses scenario earthquakes to produce a priori risk thresholds that can be referenced against current seismicity levels on an ongoing basis. Our framework is designed to inform regulatory decisions by considering the consequences of earthquake scenarios on the population and the built environment, together with simplified forecasts of the next largest magnitude. The proposed framework can tackle both the screening process needed for permitting purposes and serve as a risk management plan during operations.

Bulletin of Earthquake Engineering.

1 Introduction

Energy is essential for human civilization and development, but it also comes with environmental costs. One of these costs is induced seismicity, which refers to the earthquakes and tremors that are caused or triggered by human activities linked to energy exploration or production. Induced seismicity can pose risks to public safety and infrastructure, as well as generate public opposition and serious legal challenges to energy projects (Giardini 2009).

✉ Iason Grigoratos
iason.grigoratos@sed.ethz.ch

[1] Swiss Seismological Service (SED), ETH Zurich, Zürich, Switzerland

[2] Dutch State Supervision of Mines, The Hague, The Netherlands

[3] Department of Geoscience and Engineering, Delft University of Technology, Delft, The Netherlands

Many activities related to energy production have been linked with felt, and in very rare occasions damaging, earthquakes. Some notable examples include oil and gas extraction (Kühn et al. 2022), hydraulic fracturing (Mahani et al. 2017; Grigoratos et al. 2022), wastewater disposal (Taylor et al. 2017; Grigoratos et al. 2020), geothermal systems (Majer et al. 2007; Ellsworth et al. 2019), coal mining (Klose 2007; Li et al. 2007), natural gas storage (Vilarrasa et al. 2021), carbon storage (Goertz-Allmann et al. 2024), and hydropower dams (Foulger et al. 2018). As the world's energy needs and challenges continue to evolve, there will always be new frontiers in energy exploration and production that require new or unconventional solutions. These solutions may involve exploring new regions, tapping new resources, developing new technologies, or scaling up existing ones. However, these solutions may also come with increased induced seismic hazard levels, as they may introduce new sources of stress or imbalance to the Earth's crust. Therefore, the risks from induced seismicity will remain a persistent and complex issue that needs to be managed, to avoid constraining our potential when it comes to harnessing the Earth's resources.

An important first step is to quantify the undesirable consequences of the potential seismicity, which include human losses, physical damage to buildings and infrastructure, interruption of business and social activities, and the direct and indirect costs associated with such outcomes (Bommer 2022). Seismic risk analysis (SRA) is very often divided into deterministic (DSRA) and probabilistic analysis (PSRA). The primary difference is related to the treatment of the uncertainty behind the seismic sources. A so-called deterministic model assumes a limited set of known "active" faults that can host so-called "maximum credible earthquakes" of specific (conservative) size. Conversely, a probabilistic analysis takes into account all possible (known or unknown) faults and the entire range of plausible rupture sizes they can host. The probabilistic framework has been used at varying degrees of complexity for the Groningen gas field (Crowley et al. 2019; van Elk et al. 2019), for an Enhanced Geothermal System in Basel (Mignan et al. 2015), and for large-scale wastewater-disposal activities in Oklahoma (Gupta and Baker 2019; Grigoratos et al. 2021). Scenario-based risk calculations have been conducted for a HF sequence in the UK (Edwards et al. 2021) and for a CO_2 injection site in Switzerland (Schultz et al. 2024).

One of the key factors preventing a fully quantitative and uniform risk approach to induced seismicity management is the source model. Forecasts of earthquake-rates can vary significantly depending on the modeling assumptions, data availability, subsurface geology, human activities, and the effective triggering mechanisms (e.g., pressure, poroelastic, thermal, viscoplastic). In some special cases, it may be possible to adapt a previously calibrated model to a nearby operation; for example, under the conditions that the reservoir setting and anthropogenic source are similar. However, as new technologies emerge (e.g., enhanced geothermal systems, carbon capture and storage), there will always be cases where no applicable analogues have been tested or verified yet. Because of this limitation, risk management plans that avoid a detailed description of the source could be preferable - filling an interim niche, until sufficient source information can be gathered to suitably calibrate the forecast models.

In some sense, traffic light protocols (TLPs) are a risk management system that is agnostic of seismic source modeling. Classic TLPs outline a series of magnitude thresholds that dictate how an operation can proceed: with green-light allowing for unrestricted operations, yellow-lights requiring mitigation strategies to be enacted, and red-lights indicating the operational endpoint. These magnitude thresholds are usually selected by the regulator

as a proxy for certain levels of risk that are deemed unacceptable. The first TLP was implemented at a geothermal project at Berlín in El Salvador (Bommer et al. 2006) and similar ones have since been used in a wide variety of regions and operational settings (Bachmann et al. 2011; Kao et al. 2018; Ader et al. 2020). While TLPs have critiques (Baisch et al. 2019; Roy et al. 2021), they remain an important regulatory tool to pre-emptively define operational endpoints. Recent research has focused on better defining red-light thresholds by using quantifiable risk-based methods (Schultz et al. 2021a, b, 2022b, 2023), accounting for trailing seismicity (i.e., earthquakes that continue to occur after the operation ends) (Verdon and Bommer 2020; Schultz et al. 2022a), and incorporating real-time information (Mignan et al. 2017). These concepts have recently been expanded to fit within seismic risk guidelines (Muntendam-Bos et al. 2015; van Thienen-Visser et al. 2018; Zhou et al. 2024) for permitting gas production wells in the Netherlands (Grigoratos et al. 2023).

In the present study, we present a seismic risk protocol that is sufficiently generic to be applicable to any energy production site that has the potential to induce seismicity. Our approach fills an interim niche, until suitable source models can be developed. We also cite suitable relevant models from the literature that can be used to facilitate the necessary computations. Our recommendations are tailored to the needs of regulators and can be used both for permitting purposes and during the operational phase of a project. In other words, it can be used as a screening tool to check whether a more detailed SRA study is required and as a risk mitigation tool during operations. That said, operators can also utilize this framework either for the a priori risk assessment of a candidate site or to inform mitigation measures during operations. Our methodology follows the principles and components of PSRA, with simplifications made only regarding the seismic source. The main novelty introduced here is the dynamic estimation of the next largest earthquake based on the largest observed event and the estimated maximum magnitude. This enables us to distil the complicated probabilistic outputs of the SRA down to a basic TLP structure.

2 Methodology

In this section, we describe the components of the PSRA that our framework dictates, relevant computational methods, potential decision variables and the inversion of the static magnitude thresholds based on the PSRA outputs.

2.1 Earthquake recurrence model

The accuracy of earthquake recurrence forecasts depends heavily on modelling assumptions, data-availability, local geological conditions, and the types of triggering mechanisms involved. History has shown that scientific consensus is difficult to achieve and the dispersion in the numerical estimates can vary greatly. For example, there are several seismological models that investigated the interplay between fluid extraction, subsurface deformation, and induced seismicity in the Groningen gas field (Kühn et al. 2022). Dempsey and Suckale (2017) considered various physical processes such as poroelasticity, Coulomb failure criteria and frictional slip to probabilistically forecast felt seismicity on the 325 largest reservoir faults. However, their forecast underestimated the observed felt seismicity rate and a few years later they had to update it replacing, among other things, the fracture-mechanics

earthquake simulator with empirical magnitude-frequency distributions (Dempsey and Suckale 2023). Bourne et al. (2014) based their seismological model on the changes in reservoir volume (compaction) and assumed proportionality between the seismic moment and the total strain. The compaction model had to be calibrated using various geodetic data. This approach was later modified by Bourne and Oates (2017) to include Coulomb stresses induced by reservoir depletion. Candela et al. (2019) combined the Coulomb stressing rate with the rate-and-state friction theory (Dieterich 1994) taking into account the poroelastic effect of the differential compaction due to fault offsets. They demonstrated that this approach outperformed the traditional Coulomb failure model. This was validated also by Richter et al. (2020) who followed a similar approach and emphasized the ability of rate-and-state friction to reproduce delays in the onset of seismicity. Evidently, both the modelling approaches and the forecasts evolved greatly over time, showcasing the complexity of the problem at hand. In other words, even if consensus on source modeling methods was to be established, uncertainties in site-specific parameters can propagate into detrimentally large uncertainties in risk estimates. Thus, there is a clear need for a source-agnostic protocol that does not rely on specific seismological models and can be applied to any human activity and region.

Given that an operator may submit a permit-request with little to no in situ seismicity data available, a detailed seismic source model cannot be derived. To be pragmatic, we aim to capture in a probabilistic way the next largest earthquake that might be triggered due to the human activity in question. To that end, we first define a range of possible magnitudes; M_1 is the lower bound, M_2 is the upper bound.

We propose the following approach to start circumventing the need for a complete source model. For the lower bound, M_1 is defined as the largest observed magnitude credibly linked to the operation (regardless if the earthquake is tectonic or induced). To be on the conservative side, if no magnitudes above the magnitude of completeness (M_c) have been observed, then M_1 is set equal to M_c. M_c is the magnitude above which the overwhelming majority of earthquakes are reported in the available catalog. We should note that if the seismic network has undergone significant changes over time, then this uncertainty should be reflected in the starting choice of the time-dependent M_c. When associating nearby events to the site, one should take into account the epicentral uncertainties (across time) plus a buffer distance that implies that the stress-state within that zone is similar.

For the upper bound, M_2 is defined as the largest possible magnitude that can occur given the local geology, past historical seismicity, and the scale of human intervention. One constraint on M_2 is the size and interconnectivity of the local favourably oriented fault network and the expected stress drop. Empirical fault-scaling relations (e.g. Leonard 2014) infer the magnitude of an earthquake given the geometry and focal mechanism of a given rupture. Notably, these empirical relations have been derived from moderate to large magnitude earthquakes, with deeper hypocenters than the ones expected at energy production sites. It is likely that the relations overestimate the magnitude of small and/or shallow faults. Another constraint on M_2 is the severity of the human input. For fluid injection activities, M_2 may be limited by the size of the rock volume perturbed by pore pressure (Shapiro et al. 2013) or the total injected fluid volume (McGarr 2014; Galis et al. 2017). The method by Shapiro et al. (2013) requires data from at least one local stimulation, while Galis et al. (2017) require as input four geomechanical properties of the reservoir. The method of McGarr is the easiest to apply, but is also the least site-specific (Kwiatek et al. 2024). For fluid extraction activi-

ties, M_2 could be limited by the fraction of energy accumulated by compaction that can be seismically released (SodM, 2016; Bourne et al. 2014). In any case, given the large uncertainty behind such estimations, expert judgement will be required to assess the final value or distribution of M_2. We should note that in theory this value can also be infinite (unbounded magnitude distribution); our approach is applicable for any value of M_2.

By defining M_1 and M_2, we bound the magnitude of the next critical earthquake somewhere between the largest recorded event and the largest possible event. Obviously, under this framework, underestimating the true M_c across time can lead to underestimation of the modeled scenario magnitude. Notably, if the measurement uncertainty behind the computed magnitude solutions is non-negligible (e.g. above 0.1 magnitude units), then it must be taken into account by conservatively adjusting M_c and M_1 (towards larger values).

Next, assuming a binning of 0.1 for the range of magnitudes, one can calculate for any site the risk metrics of choice for every binned magnitude value. The focal depth and focal mechanism can be informed by local site conditions.

We should clarify that these discrete magnitudes within the range do not exhibit the same likelihood of occurrence. The likelihood that the scenario earthquake will have a given size decreases with magnitude. This is captured by a normalized Gutenberg-Richter magnitude-frequency distribution (GR-MFD), doubly truncated between a magnitude interval defined by M_1 and M_2 (Fig. 4). The probabilistic treatment is applied to the risk outputs after the fact and not at the seismic source level. This post-processing probabilistic scheme is described in Sect. 2.8.

2.2 Ground shaking intensities

Once a potential earthquake source is identified, the next step is to estimate the level of ground motion at a given location, based on that source. The primary predictor variables are usually: magnitude, distance to the rupture, and site characterization (Boore et al. 1997). Usually, the output of a Ground Motion Prediction Model (GMPM) is a certain Intensity Measures (IMs) such as the spectral acceleration at different periods (e.g., 0.01 to 10s), peak ground velocity (PGV), peak ground acceleration (PGA) or Arias intensity.

Applicable GMPM should have been calibrated with earthquake data compatible with the selected M_{min} and M_{max} values for the SHRA. They should also be compatible with the tectonic regime and focal depth of the site. Calibration of the stress drop values adopted by the GMPM would be ideal, if possible. Induced earthquakes do not appear to have significantly different stress drop than tectonic ones (Huang et al. 2017), therefore GMPM from tectonic earthquakes are valid candidates overall. Site-specific GMPM should be derived when rich seismic datasets are available. Hybrid GMPM (e.g. Edwards et al. 2018) that combine recorded ground motion data with 3D representations of Earth's structure in conjunction with dynamic kinematic representations of the earthquake source are also a viable alternative.

GMPMs are inherently limited by the scarcity of data related to large shaking amplitudes, and/or near-source recordings. This is particularly challenging for stable continental regions, where low seismicity rates and typically sparse seismic networks exacerbate the lack of data (Gerstenberger et al. 2020). As far as induced events are concerned, due to their triggering process, they are likely to be of smaller magnitude and at shallower focal depth than typical tectonic earthquakes (Grigoratos et al. 2021). The focal depths of potentially

induced events generally lie within the upper 6 km of the crust, making the seismic wave propagation more dependent on the heterogeneous properties of the uppermost crustal layers (Bommer et al. 2016).

To address these issues, several studies have developed region- or even sequence-specific GMPM for energy production related activities. Novakovic et al. (2018; 2020) and Zalachoris and Rathje (2019) developed GMPMs from data linked to wastewater disposal in Central US; Douglas et al. (2013) for low-magnitude earthquakes from geothermal areas in Europe; Sharma et al. (2013) for the Geysers Geothermal Area (USA), Edwards et al. (2018) for the Basel sequence (Switzerland), Sharma et al. (2022) for the St. Gallen sequence (Switzerland), and Cremen et al. (2020) for the Preston New Road HF sequence (UK). Finally, there are several GMPMs related to fluid-extraction based on the Groningen data (Bommer et al. 2016, 2017, 2022a, b; Paolucci et al. 2020).

Notably, when Cremen et al. (2020) tested the model by Douglas et al. (2013) against the Preston New Road data, the fit was not satisfactory despite the broad similarities in magnitude range and focal depth. Furthermore, Grigoratos et al. (2021) demonstrated that even relations developed from similar datasets can exhibit very different attenuation functions, leading to great variability in the seismic risk results (Fig. 1). Therefore, it is very difficult to confidently select a GMPM unless it can be re-calibrated or at least tested against local data.

To deal with uncertainty, it is common practice to combine multiple GMPMs via logic trees (Bommer and Scherbaum 2008; Bommer 2012; Mak et al., 2017). Beyond the use

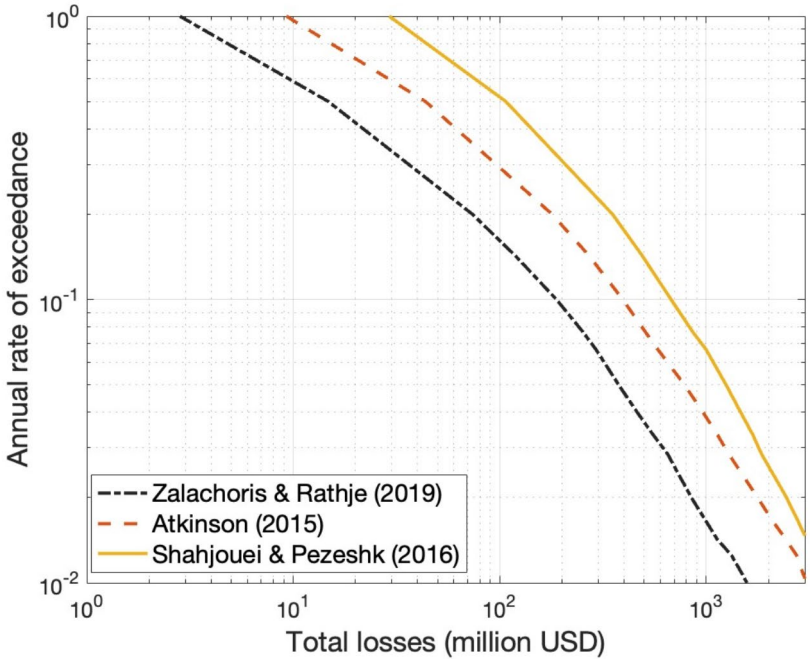

Fig. 1 Sensitivity of loss estimates from induced seismicity in the state of Oklahoma to the GMPM. The risk model is taken from Grigoratos et al. (2021) and the results are for the year 2015 and for V_{S30} 760 m/s. The losses include structural and non-structural elements and contents for all buildings in the state

of multiple GMPMs, the scaled backbone approach (Bommer 2012; Atkinson and Adams 2013; Atkinson et al. 2014a; Douglas 2018) provides an alternative for handling the wide range of uncertainties. In this approach, one GMPM is typically used to generalize the attenuation and magnitude-scaling behavior required for a specific tectonic region type for a range of magnitudes and distances.

Furthermore, Intensity Prediction Models (IPMs) can be used to estimate Intensity Scales (e.g. modified Mercalli intensity; MMI;) for a given set of earthquake magnitudes and site distances. Unlike other intensity measures such as SAs (spectral accelerations) or PGA, MMI depends solely on observations, such as felt intensities and structural damage (Wood and Neumann 1931). Therefore, the dataset used in their regression is a key factor for their applicability. Due to their empirical and generic nature, it is challenging to pair IPMs with specific exposure and fragility models, nor do they usually explicitly account for soil effects or focal mechanism.

Popular IPMs have been developed by Atkinson and Wald (2007), later revised by Atkinson et al. (2014b), focusing on North American data above M 3. Allen et al. (2012) developed a globally applicable IPM based on earthquakes with $Mw > 5$ for active crustal regions. Ahmadzadeh et al. (2020) developed an IPM for Iran, Le Goff et al. (2014) one for Portugal, Baumont et al. (2018) one for France, and Dowrick and Rhoades (2005) one for New Zealand. With the possible exception of Baumont et al. (2018), none of the aforementioned IPMs is easily applicable to very shallow small-magnitude earthquakes. A better fit for typical cases linked to energy production would be the IPM by Teng et al. (2022), which is based on likely-induced earthquakes related to wastewater disposal in Texas, Oklahoma and Kansas, with magnitudes between M 1.5 and 3.5 and hypocentral distances within 30 km. Alternatively, one could compute PGV or PGA estimates using an applicable GMPM, and then convert those to MMI using the conversion-relations of Schultz et al. (2021c), originally derived for Central and Eastern US. That said, doubling the number of conversion-steps increases considerably the uncertainty of the final output, making this solution relatively suboptimal.

2.3 Site-response

The influence of near-surface geology on seismic ground motion amplification is well-established. This phenomenon, known as seismic site response or site effects, significantly impacts amplitude and frequency content, thereby playing a crucial role in seismic hazard assessments. Site response determination relies on shear-wave velocities and lithological conditions in the shallow subsurface. Notably, many studies incorporate site response only via the V_{S30} proxy that is used as an input variable in many GMPMs. However, a number of studies have highlighted the limitations of using only V_{S30} (Derras et al. 2014; Lee and Trifunac 2010; Stewart et al. 2014). Recent efforts, like the SERA (Seismology and Earthquake Engineering Research Infrastructure Alliance for Europe) project, advocate for a more comprehensive approach. SERA recommends indicators such as fundamental resonance frequency (f_0), S-wave velocity profile ($V_s(z)$, V_{S30}, depth of seismological and engineering bedrock, surface geology, and soil class. The SERA approach surpasses traditional V_{S30} use, addressing shortcomings and providing a repository for site characterization analysis, enhancing the European Seismic Risk Model (ESRM20; Weatherill et al. 2020; 2023). In regions without direct ground motion records, the Horizontal-to-Vertical

Spectral Ratio (HVSR) of ambient vibration recordings emerges as a valuable tool for site response assessment (Bonnefoy-Claudet et al. 2006; Nakamura 1989). The HVSR identifies the fundamental resonance frequency of a soft layer over harder bedrock and thus indicates subsurface features and local variations, offering insights into seismic wave amplification.

Detailed studies are also available in some regions. In the Netherlands, for example, the unconsolidated top sedimentary layer poses a significant risk of earthquake amplification. Van Ginkel et al. (2022) developed a seismic site-response zonation map for the Netherlands (Fig. 2), using high-resolution 3D lithological sequences as proxies. Amplification Factors (AF) for each soil class are established based on empirical relationships between earthquake and HVSR records measured in the Groningen borehole network. The map categorises the country into five soil classes, each assigned an AF, which can be added to input seismic responses that conform to the reference seismic bedrock conditions. The zonation map is applicable to regions with shallow (< 3 km) induced earthquakes without a strong low-frequency (< 1.0 Hz) component. Van Ginkel et al. (2022) assessed site-response as a linear process, since the earthquake magnitudes are too low to generate non-linear site effects.

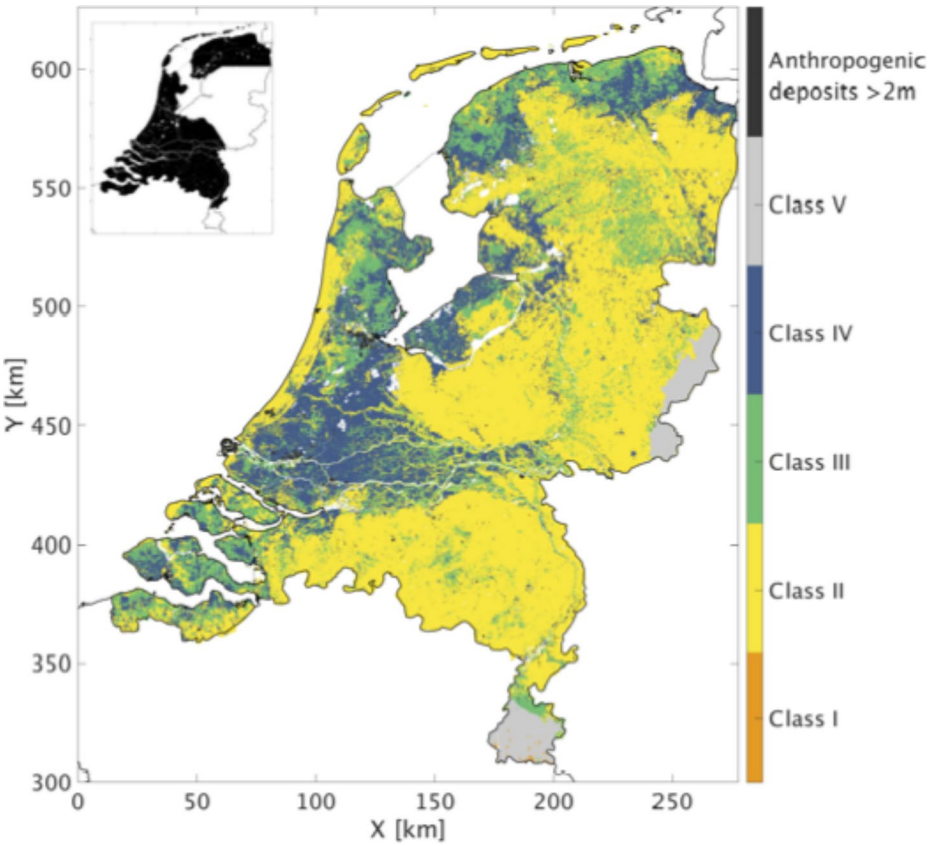

Fig. 2 Seismic site-response zonation map for the Netherlands designed for low-magnitude induced earthquakes. Each color represents a soil class with an amplification factor assigned. ©KNMI, from van Ginkel et al. (2022). This work is distributed under the Creative Commons Attribution 4.0 License

2.4 Exposure

Next, it is important to understand which assets are exposed to the seismic hazard. These assets can be, for example, residential or industrial buildings, special buildings (e.g. schools, hospitals), roads, or critical infrastructure (e.g. bridges, pipelines, energy plants, dams, ports). Each asset has its own fragility against seismic loads and its own replacement cost. Individuals are also exposed entities, although their vulnerability is dependent on the structure they reside at the time of the earthquake. These assets are aggregated at different spatial resolutions depending on data availability. Notably, the spatial resolution itself can have an impact on the loss estimates (Dabbeek et al. 2021).

The buildings in the exposure model are classified according to their seismic performance using a building taxonomy that is based on international standards (e.g. the GEM Building Taxonomy, Brzev et al. 2013; as updated by Silva et al. 2018) that allows buildings to be classified according to a number of structural attributes. The main attributes that have been selected for the consistent definition of building classes are as follows:

- Main construction material (e.g. reinforced concrete, unreinforced masonry, reinforced/confined masonry, adobe, steel, timber).
- Lateral load resisting system (e.g. infilled frame, moment frame, wall, dual frame-wall system, flat slab/plate or waffle slab, post and beam).
- Number of stories.
- Seismic design code level (pre-code, low, moderate, high).
- Lateral force coefficient used in the seismic design.

Each building typology is paired with a corresponding value for non-structural elements (e.g. mechanical equipment, windows, cladding) and contents (e.g. furniture). The occupants of each (residential) building are also part of an exposure dataset. Furthermore, special assets like bridges, dams, pipelines may also have their own, less standardized, taxonomy classes (FEMA, 2013).

The SRA should take into account the entire structural portfolio and population that is expected to undergo substantial shaking levels. For moderate to large earthquakes, this usually implies a radius of at least 100 km and 200 km for the structures and the population, respectively. Special considerations regarding dams and nuclear plants should also be warranted. We recommend adopting the lowest grid resolution possible (taking into account also the site-response model), with indicative values ranging from 1 to 5 km (Papadopoulos et al. 2024).

Depending on the region, the exposure database could be compiled in an ad hoc fashion (e.g. from census or government data). That said, a recent global compilation from GEM could also be utilized (Yepes-Estrada et al. 2017, 2023; Crowley et al. 2020), at least for the building data, if the lowest available spatial resolution meets the needs of the project. It contains information regarding structural and non-structural elements, contents and occupancy.

2.5 Fragility and vulnerability

Under ground shaking, an exposed structure will potentially sustain a certain level of damage (fragility) which will require a certain replacement cost (vulnerability). Notably,

depending on the risk metric targeted by the analysis, there is a minimum magnitude (M_{min}), below which there is no engineering interest (Bommer and Crowley 2017). In other words, the shaking is too short (in duration) or limited in frequency-content to cause any damage to the relevant structures, even at close distances. This M_{min} value represents the lower truncation of the magnitude-frequency distribution in the classical Probabilistic Seismic Hazard Analysis (PSHA) formulation. Furthermore, if the scenario earthquake adopted by the Deterministic Seismic Hazard Analysis (DSHA) or the M_{max} in PSHA is lower than $M_{min,}$ then no calculations are needed for the specific risk-metric in question.

Naturally, structural damages require a slightly larger M_{min} than non-structural damages, with the latter requiring a significantly larger M_{min} than nuisance calculations. When it comes to damages, the representative seismic design code level of the built environment plays a crucial role in determining a suitable M_{min} value. For example, the M_{min} value for structural damages in Groningen in the Netherlands (no seismic code penetration) should be much lower than the one in Japan (very high seismic code and adoption levels). Although exceptions may apply, typical indicative values for M_{min} are: 4 to 5 for structural damages (and fatalities), 3.5 to 4.5 for non-structural damages and 2 to 3 for nuisance estimates (Nievas et al. 2019; Schultz et al. 2021c). That said, in practice, a uniform M_{min} value is usually selected for both structural and non-structural damages, with a different one only for nuisance.

Any SRA assigns to each class of structure in its inventory a specific fragility (or vulnerability) curve that estimates the probabilistic distribution of damages (or losses) that this structure is expected to experience when subject to ground motions of different intensity. For the damages, modelers use standardized damage-states as labels, with typical cases being “light damage”, “significant damage”, “heavy damage”, and “collapse”. The direct economic losses are measured in terms of loss ratio, which is defined as the ratio of cost of repair to cost of replacement. Other types of losses might include population displacement, fatalities or injuries. Indirect economic losses (such as business interruption or economic disruptions) are more difficult to model and are often neglected, even though they can be very important (Sousa et al. 2022; Markhvida and Baker 2023). The IMs are usually related to the fundamental period of the structure (Silva et al. 2019), for example 5% damped pseudospectral accelerations (SA) at 0.3s. That said, in recent years, more advanced IMs are gaining traction (Kohrangi et al. 2016).

Established sources of fragility and vulnerability models are GEM (Martins and Silva 2020; Martins et al. 2021; Fig. 3) and FEMA (2013), but there are also numerous individual studies that have produced curves for specific structural typologies (e.g. Kallioras et al. 2019). Importantly, the adopted fragility curves should be compatible with the selected M_{min}.

Notably, most fragility and vulnerability functions were developed for large (tectonic) events, at least larger than magnitude 5, and hence they might be biased towards higher loss estimates, compared to the short duration and high-frequency content of induced motions. In general, these functions also ignore damage accumulation effects that might occur when buildings are subjected to a series of earthquakes (Papadopoulos et al. 2020). If more than one reliable fragility model is available for the exposed assets in question, a logic-tree approach can be applied there as well to cover the epistemic uncertainty.

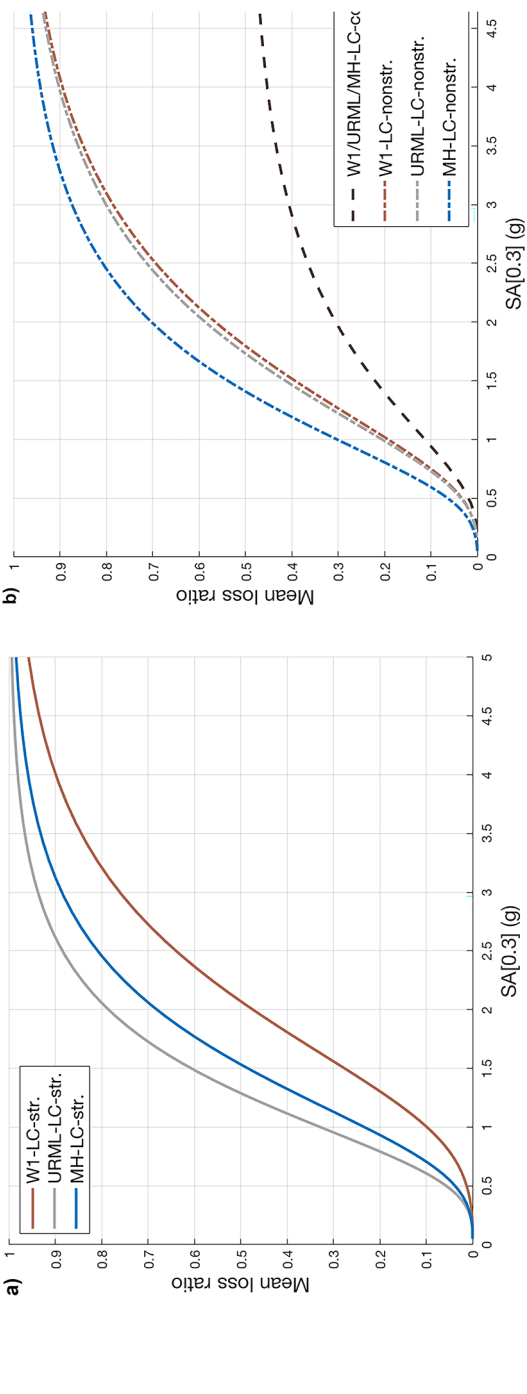

Fig. 3 Vulnerability functions for the three main building types in Oklahoma, that is, light wood frames (W1), unreinforced masonry bearing walls (URML) and mobile homes (MH). (a) Values for the structural elements (str.) are shown. (b) Values for the nonstructural (nonstr.) elements and the contents (cont.) are shown. All the curves on this figure correspond to low-code (LC) residential buildings. The curves have been produced by GEM, in collaboration with the USGS. Figure from Grigoratos et al. (2021)

2.6 Risk metrics

We propose the following risk-metrics as decision variables for whether activities at an energy production site should be deemed too risky or not by a regulator or an operator:

- aggregate nuisance level: mean total number of people feeling an earthquake (equivalent MMI scales above III).
- aggregate structural damages: mean total number of structures with at least "moderate" structural damages.
- aggregate non-structural damages: mean total number of structures with at least "severe" non-structural damages.
- local personal risk: mean probability of fatality for a person, who is continuously present without protection inside a building.

The damage-states ("light", "moderate", "severe") adopted by the global risk map of GEM (Silva et al. 2020) or those from HAZUS (FEMA 2013) could be used as reference points. Furthermore, these risk metrics refer to the entire duration of the human activity in question. Obviously, if a human activity is to be repeated multiple times (e.g. several stimulations over a number of months) then this should be taken into account with further aggregation of the results.

Ideally, inclusion of some of these metrics as well as specific tolerance thresholds would be outlined by regulatory authorities or legislation. In cases where tolerances are not previously identified, we propose that prior contextually relevant operation-ending earthquakes could be used as a benchmark. Such events (e.g. Huizinge in the Netherlands, Basel in Switzerland) often cause extensive unrest in the public, potentially damages and eventual project termination, so escalation criteria should ensure the avoidance of similar levels of risk. Often stopping well before such levels of risk have materialised might be advantageous. Thus, safety factors could be applied to further scale down the tolerance thresholds. Values between 30% and 60% for such safety factors could be reasonable; however, further site-specific sensitivity analysis should inform this choice. Notably, actual damages or damage claims associated with these events might differ from modelled risk estimates (Giardini 2009). To ensure a fair comparison, we recommend using the latter to constrain tolerance. These modelled risk estimates should be computed using equivalent model components (e.g. GMPMs, exposure data, site-amplification factors, fragility/vulnerability functions) and workflow.

2.7 Computational methods for the SHRA

The computational framework of a SHRA (Crowley and Bommer 2006) is summarized here, with more details available in Grigoratos et al. (2021). For each simulated rupture one generates many random fields of ground motion intensity measures (IMs). The random fields are then used as input to the fragility model to estimate the damage severity at any given structure for the given rupture. Next, the loss for the entire portfolio of structures is estimated by simple summation. This procedure is repeated for all random fields of each simulated rupture. Finally, the rate of exceeding any portfolio loss is empirically found by keeping track of the number of exceedances occurring over all the simulated realizations.

This approach also allows for implementation of spatial correlation between ground shaking at multiple sites from the same earthquake (Jayaram and Baker 2009), due to common source and wave traveling paths and to similar distance to fault asperities. Incorporating spatial correlations improves the reliability of the risk estimates when dealing with spatially distributed structural portfolios (Park et al. 2007).

Mandating that every operator performs the proposed seismic risk calculations, which admittedly have significant computational complexity and require familiarity with specialised software engines, seems undesirable. To address this issue, we propose that the regulator hires experienced practitioners to precompute tables of risk outputs covering every scenario rupture envisioned by the proposed protocol (Fig. 6). This task is simpler than it looks at first glance. The location of the site in question will be known, while the magnitude range of the scenario earthquakes is finite. The exposure and fragility/vulnerability models remain static. Thus, automating the whole process is straightforward. The only task the operator has to execute is to extract the right values from the risk tables (based on M1, M2), and then post-process the risk metrics according to Sect. 2.8. The risk tables could be available on spread-sheets, and both the data-mining and the weighting scheme could be done with simple predetermined input functions.

2.8 Probabilistic expression of the next largest magnitude

The prior sections describe a workflow to estimate risk metrics for possible earthquake scenarios at a given location. From this point, we define a post-processing workflow that allows for an estimation of risk from the hypothetical next largest earthquake scenario and the subsequent decision-making criteria. We begin by considering a (normalized) Gutenberg-Richter magnitude-frequency distribution (GR-MFD), doubly truncated between a magnitude interval of M_1 and M_2 (Fig. 4; Schultz 2024). Here, M_1 is the lower magnitude bound, M_2 is the upper magnitude bound, and b is the GR-MFD b-value providing the proportionality between bigger and smaller events. Note that M_1 is a dynamic variable that might change during an operation, if larger events are sequentially observed. In theory, M_2 might also change if, for example, the planned operations are altered (e.g. different cumulative injected volume), or if larger faults or higher stress drops are identified. The normalized GR-MFD can be used to define the probability density function (PDF) and the cumulative distribution function (CDF). In this sense, we can bound the likelihood of the next largest event's magnitude– somewhere between the current largest observed event (M_1) and the estimate of the largest possible event (M_2). The b-value can be informed by prior suitable cases of the same human activity (via a logic-tree approach), or from nearby tectonic events (ideally of similar depth). This PDF is used as an alternative to the seismic source: each (precomputed) risk output can be weighted according to the (normalized) PDF of its source-magnitude (for more details see Sect. 2.9). In the end, by simple bookkeeping, a probabilistic distribution is obtained for each considered risk metric (Sect. 2.6).

For illustration purposes, we provide a simplified example to demonstrate this post-processing workflow (Fig. 5) partially using data from a prior study that considered induced seismicity risks in the Netherlands (Schultz et al. 2022b). From this study, scenario risk tables for nuisance, non-structural residential damages and LPR are estimated. For the dotted line, each risk estimate (y axis) corresponds to a different scenario earthquake (x axis). The severity of the risk scenarios increases monotonically as the magnitude increases. For

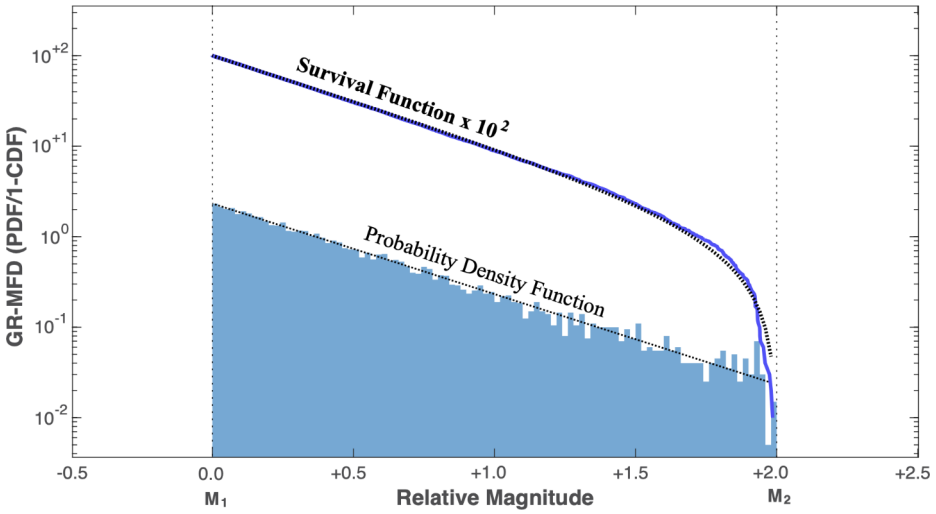

Fig. 4 Indicative example of a doubly truncated GR-MFD. The analytical PDF (thinner dashed black line) and Survival Function (1-CDF; thicker dashed black line) are shown for a doubly truncated GR-MFD with a b-value of 1.0, bounded between M_1 and M_2. As well, a randomly drawn catalogue with 10^4 events is drawn to visually compare the empirical PDF (blue bars) and survival functions (blue line). Note that the survival function has been artificially offset by a factor of 10^2 to make it visually distinct from the PDF. The expected value of the next largest magnitude is the mean of the PDF

the solid line, the GR-MFD PDF provides weights to compute an average expected risk for the next largest event (y axis), given some observed event M_1 (x axis). We arbitrarily consider here an M_2 of M_c+3.5 and a b-value of 1.2. The expected risk from the next largest magnitude increases monotonically and is always greater than the scenario risk (until reaching the upper truncation bound).

In order to use this workflow to inform decision-making, tolerances to each risk are required. For demonstration, we compare against the impacts estimated from the 2012 M_L 3.6 Huizinge event in Groningen (Fig. 5; Schultz et al. 2022b). We would want to stop operations before anticipating this level of risk, since this earthquake ended gas production operations (van der Voort and Vanclay 2015; Muntendam-Bos et al. 2022). All the considered risk metrics (nuisance, non-structural damages, and LPR) suggest that operations would need to change or stop well before an M_c +1.3 to +1.7 event has been observed. We reiterate that this is a simple example with certain arbitrary considerations constructed just to demonstrate our conceptual workflow.

2.9 Linkages to risk management plans and TLPs

We propose that our prior workflow and decision variables can be used to inform risk management plans, like the TLP. TLPs typically are stratified into three tiers as defined below.

- Green light: the maximum observed magnitude is below the yellow-light threshold (M_Y). Operations within the field continue as planned.
- Yellow light: the maximum observed magnitude is above M_Y, but below the red-light threshold (M_R). Operations continue, but the operator must enact mitigation measures

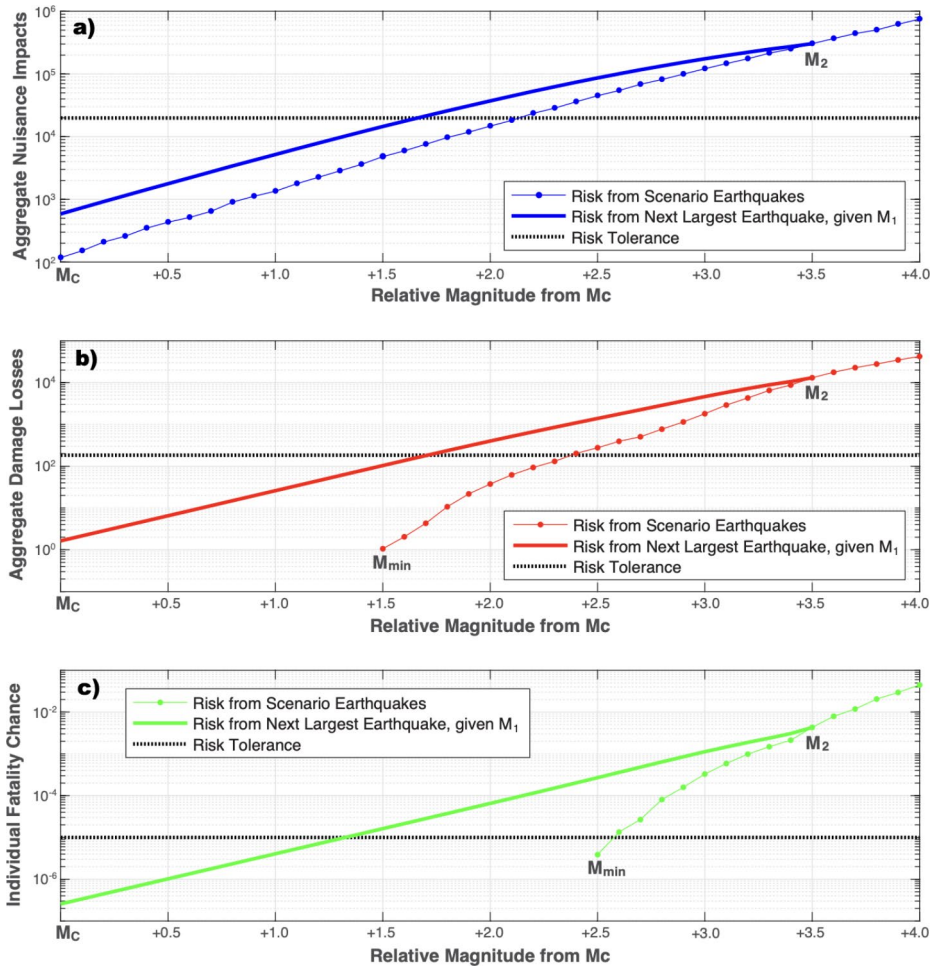

Fig. 5 Post-processing workflow example. Three metrics of risk are considered: (a) nuisance, (b) non-structural damages, and (c) LPR. In each panel, the scenario risk (thinner dotted line) is compared alongside the anticipated risk from the next largest magnitude (thicker solid line) and an estimate of the risk tolerance (dashed horizontal line). The x-axis represents either the scenario magnitude (thinner dotted line) or M_1 (thicker solid line). The two risk curves meet at $M_c + 3.5$ since this value was chosen as the upper magnitude bound M_2. Computed risk values above M_2 are only shown for illustration purposes

to limit the probability of a larger event.

- Red light: the maximum observed magnitude is above the red-light threshold (M_R). Subsurface operations must stop, at the discretion of the regulator.

We define M_R based on our framework presented in Sect. 2.1–2.8 (Fig. 6). Specifically, we first derive for each of the selected risk metrics, which magnitude value M_{cr} leads to exceedance of the agreed upon tolerances. We treat M_{cr} as the mean of the GR-MFD PDF shown in Fig. 4. With this information, for each metric, we can solve for M_1, because M_2 and the b-value are known. From this, M_R is defined as the smallest from these M_1 values.

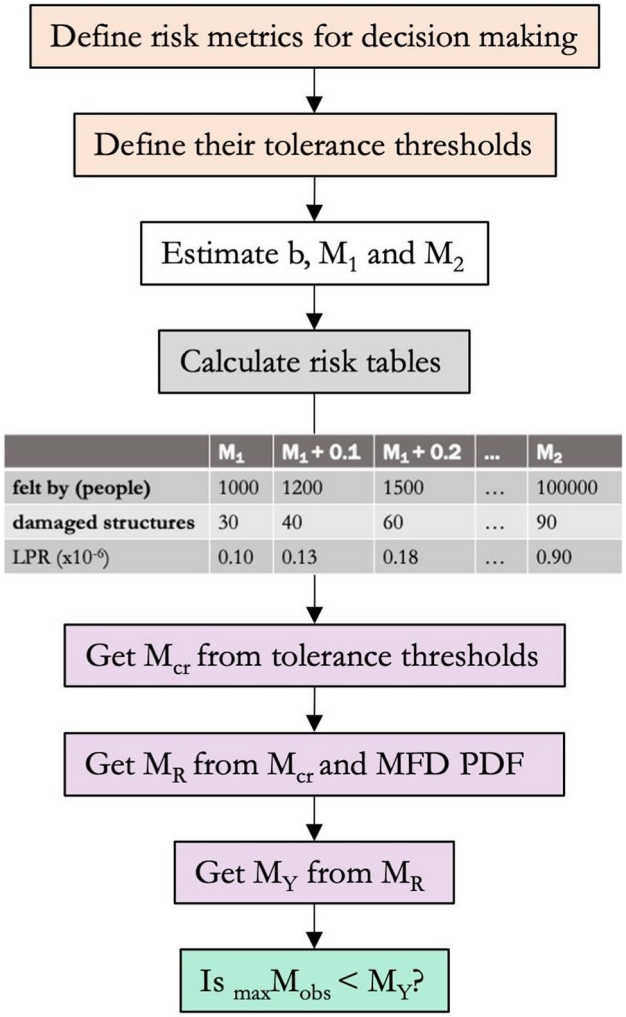

	M_1	$M_1 + 0.1$	$M_1 + 0.2$	...	M_2
felt by (people)	1000	1200	1500	…	100000
damaged structures	30	40	60	…	90
LPR ($x10^{-6}$)	0.10	0.13	0.18	…	0.90

Fig. 6 Flowchart of the risk management plan. The steps are color-coded to reflect the presence of five different modules that can be computed independently. The arrows reflect the ideal order of computations

Then, M_Y can be determined by stepping back from M_R by an amount (ΔM_{jump}) we anticipate that magnitudes could jump during an operator's mitigation. Obviously, for this plan to be operational, the M_c must be smaller than M_Y. The value of ΔM_{jump} in cases driven by fluid injection can be up to 2 magnitude units (Verdon and Bommer 2020; Schultz et al. 2022a). For other human activities this value might be smaller or larger. Further research to better constrain this variable is needed. Finally, if the measurement uncertainty behind the computed magnitude solutions is non-negligible (e.g. above 0.1 magnitude units), then it must be taken into account by conservatively adjusting M_c, M_Y and M_R (towards lower values).

3 Discussion and conclusions

As the world is gradually phasing out fossil fuels as a key energy source, new frontiers in energy exploration and production will emerge. These endeavours may require solutions that affect the balance of Earth's crust in unfavourable ways, leading to elevated levels of seismic hazard. Thus, a broader discussion is needed on the trade-offs between energy security, net-zero emission goals, and induced seismic hazard. Notably, this discussion might lead to tolerance levels (in terms of seismic risk) that depend on the importance of the energy project in question. In any case, once the tolerance levels are agreed upon, the protocol we present in this study can be used to assess the probability of exceeding them and to define a magnitude-based TLP for monitoring purposes.

Our source agnostic framework for management of induced seismicity risk is both advantageous and practical. Advantageous in the sense that risk-reducing decisions can still be made, even in the absence of a complete description of the source. This is significant, because our changing world will always be considering new subsurface resources/technologies - potentially ones without any suitable analogues for earthquake source modeling. It is also practical in the sense that this approach can be readily adapted in any jurisdiction that has pre-existing risk modeling capabilities. Our approach has been tailored to utilise the conventional outputs of scenario risk modeling (Sect. 2.1–2.7) and then translate them into decision variables based on risk tolerances and GR-MFD statistics (Sect. 2.8). Thus, these previously existing workflows can readily adapt their outputs to consider induced seismicity risk. While we have discussed the implications for informing the red- and yellow-light thresholds within a TLP (Sect. 2.9), this analysis could also be used to inform the issuing of permits or interim pre-screening.

From the start, we made the deliberate choice to render our approach source-agnostic, in order to make it widely applicable to any type of induced seismicity, in any region. One deficiency of our source agnostic approach to note is that we have not explicitly used a trailing seismicity model. This is because the existing trailing seismicity models are only calibrated on short-term cases of induced seismicity triggered by fluid-injection (Schultz et al. 2022a). If some estimates of trailing seismicity are known (Watkins et al. 2023), this information can easily be incorporated in the decision variable estimation (Sect. 2.8). On the other hand, this deficiency could also be addressed by conservatively applying a scaling factor to the risk tolerances; in this case, the approach would remain truly source agnostic. Furthermore, our framework could also be augmented with uncertainty ranges around the b-value and the M_2. A probabilistic treatment of these parameters could mimic the logic tree structure we outline for the ground shaking models. The user can determine whether this added complexity is warranted, on a case-by-case basis.

Despite its current generic form, our framework was originally designed to tackle induced seismicity related to gas production. It is based on a report commissioned by the Dutch State Supervision of Mines (SodM) (Grigoratos et al. 2023), and later reviewed by an external panel of experts with either industry or regulatory experience. It includes various implementation details regarding fluid extraction projects, especially when it comes to a priori analyses for permitting purposes. It was a preparatory study for the development of a new protocol for Seismic Hazard and Risk Assessments (SHRA) of induced seismicity related to the production of small gas fields in the Netherlands.

Finally, we should highlight the importance of seismic monitoring both before and during the operations of the energy project (Zhou et al. 2024). In the planning phase of the project, a low M_c is essential to understand the background seismic activity levels at the site, before human activities come into play. During operations, it enables the stakeholders to monitor the potential rise in observed magnitudes with a long enough lead time, enabling potential mitigation measures before the yellow or red light is reached. Crucially, the protocol-design incentivizes the operator to lower the M_c, since M_1 is set as always larger or equal to M_c.

Acknowledgements This work was funded by the Dutch State Supervision of Mines (SodM). We would like to acknowledge Shawn Maxwell, Gunter Siddiqi and an anonymous reviewer for providing feedback on the commissioned report. JvG has received research funding from the ETH Postdoctoral fellowship.

Author contributions I.G. served as the project manager. I.G. and R.S. designed the framework, conducted literature review and drafted the initial manuscript. J.v.G. and T.G conducted literature review and drafted parts of the report. S.W., J.v.d.W., and A.M.B. conceptualized the study and provided key inputs on regulatory matters. All authors reviewed and approved the final version of the manuscript.

Funding Open access funding provided by Swiss Federal Institute of Technology Zurich

Data availability The commissioned report (Grigoratos et al. 2023) is available at https://www.sodm.nl/actueel/nieuws/2024/04/19/evaluatie-van-de-tijdelijke-leidraad-voor-seismische-risicoanalyse-van-kleine-gasvelden.

Declarations

Conflict of interest No competing interests.

References

Ader T, Chendorain M, Free M, Saarno T, Heikkinen P, Malin PE, Leary P, Kwiatek G, Dresen G, Bluemle F, Vuorinen T (2020) Design and implementation of a traffic light system for deep geothermal well stimulation in Finland. J Seismolog 24(5):991–1014. https://doi.org/10.1007/s10950-019-09853-y

Ahmadzadeh S, Doloei GJ, Zafarani H (2020) New intensity prediction equation for Iran. J Seismol 24(1):23–35

Allen TI, Wald DJ, Worden CB (2012) Intensity attenuation for active crustal regions. J Seismolog 16:409–433

Atkinson GM, Adams J (2013) Ground motion prediction equations for application to the 2015 Canadian national seismic hazard maps. Can J Civ Eng 40(10):988–998

Atkinson GM, Wald DJ (2007) Did You Feel It? intensity data: A surprisingly good measure of earthquake ground motion. Seismol Res Lett 78(3):362–368

Atkinson GM, Bommer JJ, Abrahamson NA (2014a) Alternative approaches to modeling epistemic uncertainty in ground motions in probabilistic seismic-hazard analysis. Seismol Res Lett 85:1141–1144

Atkinson GM, Worden CB, Wald DJ (2014b) Intensity prediction equations for North America. Bull Seismol Soc Am 104(6):3084–3093

Bachmann CE, Wiemer S, Woessner J, Hainzl S (2011) Statistical analysis of the induced Basel 2006 earthquake sequence: Introducing a probability-based monitoring approach for Enhanced Geothermal Systems: Probability-based monitoring approach for EGS. Geophys J Int 186(2):793–807. https://doi.org/10.1111/j.1365-246X.2011.05068.x

Baisch S, Koch C, Muntendam-Bos A (2019) Traffic light systems: to what extent can induced seismicity be controlled? Seismol Res Lett 90(3):1145–1154. https://doi.org/10.1785/0220180337

Baumont D, Manchuel K, Traversa P, Durouchoux C, Nayman E, Ameri G (2018) Intensity predictive attenuation models calibrated in Mw for metropolitan France. Bull Earthq Eng 16:2285–2310

Bommer JJ (2012) Challenges of building logic trees for probabilistic seismic hazard analysis. Earthq Spectra 28:1723–1735

Bommer JJ (2022) Earthquake hazard and risk analysis for natural and induced seismicity: Towards objective assessments in the face of uncertainty. Bull Earthq Eng 20(6):2825–3069. https://doi.org/10.1007/s10518-022-01357-4

Bommer JJ, Crowley H (2017) The Purpose and Definition of the Minimum Magnitude Limit in PSHA Calculations. Seismol Res Lett 88(4):1097–1106. https://doi.org/10.1785/0220170015

Bommer JJ, Scherbaum F (2008) The Use and Misuse of Logic Trees in Probabilistic Seismic Hazard Analysis. Earthq Spectra 24(4):997–1009. https://doi.org/10.1193/1.2977755

Bommer JJ, Oates S, Cepeda JM, Lindholm C, Bird J, Torres R, Marroquín G, Rivas J (2006) Control of hazard due to seismicity induced by a hot fractured rock geothermal project. Eng Geol 83(4):287–306. https://doi.org/10.1016/j.enggeo.2005.11.002

Bommer JJ, Dost B, Edwards B, Stafford PJ, van Elk J, Doornhof D, Ntinalexis M (2016) Developing an Application-Specific Ground-Motion Model for Induced Seismicity. Bull Seismol Soc Am 106(1):158–173. https://doi.org/10.1785/0120150184

Bommer JJ, Dost B, Edwards B, Kruiver PP, Ntinalexis M, Rodriguez-Marek A, Stafford PJ, van Elk J (2017) Developing a model for the prediction of ground motions due to earthquakes in the Groningen gas field. Neth J Geosci 96(05):s203–s213. https://doi.org/10.1017/njg.2017.28

Bommer JJ, Stafford PJ, Ruigrok E, Rodriguez-Marek A, Ntinalexis M, Kruiver PP, Edwards B, Dost B, van Elk J (2022a) Ground-motion prediction models for induced earthquakes in the Groningen gas field, the Netherlands. J Seismolog 26(6):1157–1184. https://doi.org/10.1007/s10950-022-10120-w

Bommer JJ, Edwards B, Kruiver PP, Rodriguez-Marek A, Stafford PJ, Ntinalexis M, Ruigrok E, Dost B (2022b) V7 ground-motion model for induced seismicity in the Groningen gas field, Revision 1, 20 February 2022, 282 pp, available for download at https://nam-onderzoeksrapporten.data-app.nl/reports/download/groningen/en/06766b7a-1999-4f48-977c-33a5d94cdd82

Bonnefoy-Claudet S, Cotton F, Bard P-Y (2006) The nature of noise wavefield and its applications for site effects studies: A literature review. Earth Sci Rev 79(3):205–227. https://doi.org/10.1016/j.earscirev.2006.07.004

Boore DM, Joyner WB, Fumal TE (1997) Equations for estimating horizontal response spectra and peak acceleration from western North American earthquakes: A summary of recent work. Seismol Res Lett 68(1):128–153

Bourne SJ, Oates SJ (2017) Extreme threshold failures within a heterogeneous elastic thin-sheet and the spatial-temporal development of induced seismicity within the Groningen gas field. J Geophys Research: Solid Earth 122:10,299–10320. https://doi.org/10.1002/2017JB014356

Bourne SJ, Oates SJ, van Elk J, Doornhof D (2014) A seismological model for earthquakes induced by fluid extraction from a subsurface reservoir. J Geophys Research: Solid Earth 119:8991–9015. https://doi.org/10.1002/2014JB011663

Brzev S, Scawthorn C, Charleson AW, Allen L, Greene M, Jaiswal K, Silva V (2013) GEM building taxonomy (Version 2.0) (No. 2013-02). GEM Foundation

Candela T, Osinga S, Ampuero JP, Wassing B, Pluymaekers M, Fokker PA, Muntendam-Bos AG (2019) Depletion-induced seismicity at the Groningen gas field: Coulomb rate-and-state models including differential compaction effect. J Geophys Research: Solid Earth 124(7):7081–7104

Cremen G, Werner MJ, Baptie B (2020) A New Procedure for Evaluating Ground-Motion Models, with Application to Hydraulic-Fracture-Induced Seismicity in the United Kingdom. Bull Seismol Soc Am 110(5):2380–2397. https://doi.org/10.1785/0120190238

Crowley H, Bommer JJ (2006) Modelling seismic hazard in earthquake loss models with spatially distributed exposure. Bull Earthq Eng 4(3):249–273

Crowley H, Pinho R, van Elk J, Uilenreef J (2019) Probabilistic damage assessment of buildings due to induced seismicity. Bull Earthq Eng 17(8):4495–4516. https://doi.org/10.1007/s10518-018-0462-1

Crowley H, Despotaki V, Rodrigues D, Silva V, Toma-Danila D, Riga E, Karatzetzou A, Fotopoulou S, Zugic Z, Sousa L, Ozcebe S, Gamba P (2020) Exposure model for European seismic risk assessment. Earthq Spectra 875529302091942. https://doi.org/10.1177/8755293020919429

Dabbeek J, Crowley H, Silva V, Weatherill G, Paul N, Nievas CI (2021) Impact of exposure spatial resolution on seismic loss estimates in regional portfolios. Bull Earthq Eng 19(14):5819–5841. https://doi.org/10.1007/s10518-021-01194-x

Dempsey D, Suckale J (2017) Physics-based forecasting of induced seismicity at Groningen gas field, the Netherlands. Geophys Res Lett 44(15):7773–7782

Dempsey DE, Suckale J (2023) Physics-Based Forecasting of Induced Seismicity at Groningen Gas Field, The Netherlands: Post Hoc Evaluation and Forecast Update. Seismological Society of America

Derras B, Bard PY, Cotton F (2014) Towards fully data driven ground-motion prediction models for Europe. Bull Earthq Eng 12(1):495–516

Dieterich J (1994) A constitutive law for rate of earthquake production and its application to earthquake clustering. J Phys Res 99:2601–2618. https://doi.org/10.1029/93JB02581

Douglas J (2018) Calibrating the backbone approach for the development of earthquake ground motion models. Best Practice in Physics-based Fault Rupture Models for Seismic Hazard Assessment of Nuclear Installations. Issues and Challenges Towards Full Seismic Risk Analysis

Douglas J, Edwards B, Convertito V, Sharma N, Tramelli A, Kraaijpoel D, Cabrera BM, Maercklin N, Troise C (2013) Predicting ground motion from induced earthquakes in geothermal areas. Bull Seismol Soc Am 103(3):1875–1897

Dowrick D, Rhoades D (2005) Revised models for attenuation of modified Mercalli intensity in New Zealand earthquakes. Bull New Zeal Soc Earthq Eng 38(4):185–214

Edwards B, Staudenmaier N, Cauzzi C, Wiemer S (2018) A Hybrid Empirical Green's Function Technique for Predicting Ground Motion from Induced Seismicity: Application to the Basel Enhanced Geothermal System. Geosciences 8(5):180. https://doi.org/10.3390/geosciences8050180

Edwards B, Crowley H, Pinho R, Bommer JJ (2021) Seismic Hazard and Risk Due to Induced Earthquakes at a Shale Gas Site. Bull Seismol Soc Am. https://doi.org/10.1785/0120200234

Ellsworth WL, Giardini D, Townend J, Ge S, Shimamoto T (2019) Triggering of the Pohang, Korea, Earthquake (Mw 5.5) by Enhanced Geothermal System Stimulation. https://doi.org/10.1785/0220190102. Seismological Research Letters

Federal Emergency Management Agency (FEMA) (2013) Multi-Hazard Loss Estimation Methodology, Earthquake Model, Hazus-MH 2.1, Technical Manual

Foulger GR, Wilson MP, Gluyas JG, Julian BR, Davies RJ (2018) Global review of human-induced earthquakes. Earth Sci Rev 178:438–514. https://doi.org/10.1016/j.earscirev.2017.07.008

Galis M, Ampuero JP, Mai PM, Cappa F (2017) Induced seismicity provides insight into why earthquake ruptures stop. Sci Adv 3(12):eaap7528. https://doi.org/10.1126/sciadv.aap7528

Gerstenberger MC, Marzocchi W, Allen T, Pagani M, Adams J, Danciu L, Field EH, Fujiwara H, Luco N, Ma K-F, Meletti C, Petersen MD (2020) Probabilistic Seismic Hazard Analysis at Regional and National Scales: State of the Art and Future Challenges. Rev Geophys 58(2). https://doi.org/10.1029/2019RG000653

Giardini D (2009) Geothermal quake risks must be faced. Nature 462(7275):848–849. https://doi.org/10.1038/462848a

Goertz-Allmann BP, Langet N, Iranpour K, Kühn D, Baird A, Oates S, Nakstad H (2024) Effective microseismic monitoring of the Quest CCS site, Alberta, Canada. Int J Greenhouse Gas Control 133:104100. https://doi.org/10.1016/j.ijggc.2024.104100

Grigoratos I, Rathje E, Bazzurro P, Savvaidis A (2020) Earthquakes induced by wastewater injection, part II: Statistical evaluation of causal factors and seismicity rate forecasting. Bull Seismol Soc Am 110(5):2483–2497. https://doi.org/10.1785/0120200079

Grigoratos I, Bazzurro P, Rathje E, Savvaidis A (2021) Time-dependent seismic hazard and risk due to wastewater injection in Oklahoma. Earthq Spectra 37(3):2084–2106. https://doi.org/10.1177/8755293020988020

Grigoratos I, Savvaidis A, Rathje E (2022) Distinguishing the causal factors of induced seismicity in the Delaware Basin: Hydraulic fracturing or wastewater disposal? Seismological Soc Am 93(5):2640–2658. https://doi.org/10.1785/0220210320

Grigoratos I, Schultz R, van Ginkel J, Gunatilake T, Wiemer S (2023) Review of the Seismic Hazard and Risk Protocol for induced seismicity related to gas production from small gas fields in the Netherlands. SodM Report. https://www.sodm.nl/actueel/nieuws/2024/04/19/evaluatie-van-de-tijdelijke-leidraad-voor-seismische-risicoanalyse-van-kleine-gasvelden

Gupta A, Baker JW (2019) A framework for time-varying induced seismicity risk assessment, with application in Oklahoma. Bull Earthq Eng 17(8):4475–4493

Huang Y, Ellsworth WL, Beroza GC (2017) Stress drops of induced and tectonic earthquakes in the central United States are indistinguishable. Sci Adv 3(8):e1700772. https://doi.org/10.1126/sciadv.1700772

Jayaram N, Baker JW (2009) Correlation model for spatially distributed ground-motion intensities. Earthq Eng Struct Dynamics 38(15):1687–1708. https://doi.org/10.1002/eqe.922

Kallioras S, Graziotti F, Penna A (2019) Numerical assessment of the dynamic response of a URM terraced house exposed to induced seismicity. Bull Earthq Eng 17(3):1521–1552. https://doi.org/10.1007/s10518-018-0495-5

Kao H, Visser R, Smith B, Venables S (2018) Performance assessment of the induced seismicity traffic light protocol for northeastern British Columbia and western Alberta. Lead Edge 37(2):117–126. https://doi.org/10.1190/tle37020117.1

Klose CD (2007) Geomechanical modeling of the nucleation process of Australia's 1989 M5.6 Newcastle earthquake. Earth Planet Sci Lett 256(3–4):547–553. https://doi.org/10.1016/j.epsl.2007.02.009

Kohrangi M, Vamvatsikos D, Bazzurro P (2016) Implications of intensity measure selection for seismic loss assessment of 3-D buildings. Earthq Spectra 32(4):2167–2189

Kühn D, Hainzl S, Dahm T, Richter G, Rodriguez IV (2022) A review of source models to further the understanding of the seismicity of the Groningen field. Neth J Geosci 101:e11 https://doi.org/10.1017/njg.2022.7

Kwiatek G, Grigoratos I, Wiemer S (2024) Variability of seismicity rates and maximum magnitude for adjacent hydraulic stimulations. Seismological Research Letters. (in press)

Le Goff B, Borges JF, Bezzeghoud M (2014) Intensity-distance attenuation laws for the Portugal mainland using intensity data points. Geophys J Int 199(2):1278–1285

Lee VW, Trifunac MD (2010) Should average shear-wave velocity in the top 30m of soil be used to describe seismic amplification? Soil Dyn Earthq Eng 30(11):1250–1258. https://doi.org/10.1016/j.soildyn.2010.05.007

Leonard M (2014) Self-Consistent Earthquake Fault-Scaling Relations: Update and Extension to Stable Continental Strike-Slip Faults. Bull Seismol Soc Am 104(6):2953–2965. https://doi.org/10.1785/0120140087

Li T, Cai MF, Cai M (2007) A review of mining-induced seismicity in China. Int J Rock Mech Min Sci 44(8):1149–1171. https://doi.org/10.1016/j.ijrmms.2007.06.002

Mahani AB, Schultz R, Kao H, Walker D, Johnson J, Salas C (2017) Fluid Injection and Seismic Activity in the Northern Montney Play, British Columbia, Canada, with Special Reference to the 17 August 2015 Mw 4.6 Induced Earthquake. Bull Seismol Soc Am 107(2):542–552. https://doi.org/10.1785/0120160175

Majer EL, Baria R, Stark M, Oates S, Bommer J, Smith B, Asanuma H (2007) Induced seismicity associated with enhanced geothermal systems. Geothermics 36(3):185–222

Mak S, Cotton F, Schorlemmer D (2017) Measuring the performance of ground-motion models: The importance of being independent. Seismol Res Lett 88(5):1212–1217

Markhvida M, Baker JW (2023) Modeling future economic costs and interdependent industry recovery after earthquakes. Earthq Spectra 39(2):914–937

Martins L, Silva V (2020) Development of a fragility and vulnerability model for global seismic risk analyses. Bull Earthq Eng. https://doi.org/10.1007/s10518-020-00885-1

Martins L, Silva V, Crowley H, Cavalieri F (2021) Vulnerability modellers toolkit, an open-source platform for vulnerability analysis. Bull Earthq Eng 19:5691–5709

McGarr A (2014) Maximum magnitude earthquakes induced by fluid injection: Limits on fluid injection earthquakes. J Geophys Research: Solid Earth 119(2):1008–1019. https://doi.org/10.1002/2013JB010597

Mignan A, Landtwing D, Kästli P, Mena B, Wiemer S (2015) Induced seismicity risk analysis of the 2006 Basel, Switzerland, Enhanced Geothermal System project: Influence of uncertainties on risk mitigation. Geothermics 53:133–146. https://doi.org/10.1016/j.geothermics.2014.05.007

Mignan A, Broccardo M, Wiemer S, Giardini D (2017) Induced seismicity closed-form traffic light system for actuarial decision-making during deep fluid injections. Sci Rep 7(1):13607. https://doi.org/10.1038/s41598-017-13585-9

Muntendam-Bos AG, Roest JPA, de Waal JA (2015) A guideline for assessing seismic risk induced by gas extraction in the Netherlands. Lead Edge 34(6):672–677. https://doi.org/10.1190/tle34060672.1

Muntendam-Bos AG, Hoedeman G, Polychronopoulou K, Draganov D, Weemstra C, van der Zee W, Bakker RR, Roest H (2022) An overview of induced seismicity in the Netherlands. Neth J Geosci 101:e1. https://doi.org/10.1017/njg.2021.14

Nakamura Y (1989) A method for dynamic characterisation estimation of subsurface using microtremor on the ground surface. Railway Tech Res Inst Q Rep 30(1):25–33. https://trid.trb.org/view/294184

Nievas CI, Bommer JJ, Crowley H, van Elk J (2019) Global occurrence and impact of small-to-medium magnitude earthquakes: A statistical analysis. Bull Earthq Eng. https://doi.org/10.1007/s10518-019-00718-w

Paolucci R, Mazzieri I, Piunno G, Smerzini C, Vanini M, Özcebe AG (2020) Earthquake ground motion modeling of induced seismicity in the Groningen gas field. Earthq Eng Struct Dynamics eqe3367. https://doi.org/10.1002/eqe.3367

Papadopoulos AN, Bazzurro P, Marzocchi W (2020) Exploring probabilistic seismic risk assessment accounting for seismicity clustering and damage accumulation: Part I. Hazard analysis. Earthq Spectra 875529302095733. https://doi.org/10.1177/8755293020957338

Papadopoulos AN, Roth P, Danciu L (2024) Exposure manipulation strategies for balancing computational efficiency and precision in seismic risk analysis. Bull Earthq Eng 37(2). https://doi.org/10.1177/8755293020957338

Park J, Bazzurro P, Baker JW (2007) Modeling spatial correlation of ground motion intensity measures for regional seismic hazard and portfolio loss estimation. Appl Stat Probab civil Eng 2:1–8

Richter G, Hainzl S, Dahm T, Zöller G (2020) Stress-based, statistical modeling of the induced seismicity at the Groningen gas field, The Netherlands. Environ Earth Sci 79(11):252

Roy C, Nowacki A, Zhang X, Curtis A, Baptie B (2021) Accounting for Natural Uncertainty Within Monitoring Systems for Induced Seismicity Based on Earthquake Magnitudes. Front Earth Sci 9:634688. https://doi.org/10.3389/feart.2021.634688

Schultz R (2024) Inferring maximum magnitudes from the ordered sequence of large earthquakes. Philosophical Trans Royal Soc A: Math Phys Eng Sci. https://doi.org/10.1098/rsta.2023.0185

Schultz R, Beroza GC, Ellsworth WL (2021a) A Strategy for Choosing Red-Light Thresholds to Manage Hydraulic Fracturing Induced Seismicity in North America. J Geophys Research: Solid Earth 126(12). https://doi.org/10.1029/2021JB022340

Schultz R, Beroza GC, Ellsworth WL (2021b) A risk-based approach for managing hydraulic fracturing–induced seismicity. Science 372(6541):504–507. https://doi.org/10.1126/science.abg5451

Schultz R, Quitoriano V, Wald DJ, Beroza GC (2021c) Quantifying nuisance ground motion thresholds for induced earthquakes. Earthq Spectra 875529302098802. https://doi.org/10.1177/8755293020988025

Schultz R, Ellsworth WL, Beroza GC (2022a) Statistical bounds on how induced seismicity stops. Sci Rep 12(1):1184. https://doi.org/10.1038/s41598-022-05216-9

Schultz R, Muntendam-Bos A, Zhou W, Beroza GC, Ellsworth WL (2022b) Induced seismicity red-light thresholds for enhanced geothermal prospects in the Netherlands. Geothermics 106:102580. https://doi.org/10.1016/j.geothermics.2022.102580

Schultz R, Baptie B, Edwards B, Wiemer S (2023) Red-light thresholds for induced seismicity in the UK. Seismica 2(2). https://doi.org/10.26443/seismica.v2i2.1086

Schultz R, Rinaldi AP, Roth P, Madritsch H, Gunatilake T, Wiemer S (2024) Pre-screening of induced seismicity risks for CO2 injection at Trüllikon, Switzerland. Int J Greenhouse Gas Control 138:104239

Shapiro SA, Krüger OS, Dinske C (2013) Probability of inducing given-magnitude earthquakes by perturbing finite volumes of rocks. J Geophys Research: Solid Earth 118(7):3557–3575. https://doi.org/10.1002/jgrb.50264

Sharma N, Convertito V, Maercklin N, Zollo A (2013) Ground-Motion Prediction Equations for The Geysers Geothermal Area based on Induced Seismicity Records. Bull Seismol Soc Am 103(1):117–130. https://doi.org/10.1785/0120120138

Sharma N, Convertito V, De Matteis R, Capuano P (2022) Strong ground-motion prediction equations from induced earthquakes in St. Gallen geothermal field, Switzerland. J Geophys Eng 19(4):820–832. https://doi.org/10.1093/jge/gxac044

Silva V, Yepes-Estrada C, Dabbeek J, Martins L, Brzev S (2018) GED4ALL: Global exposure database for multi-hazard risk analysis —Multi-hazard exposure taxonomy. GEM technical report 2018-01. Pavia: GEM Foundation

Silva V, Akkar S, Baker J, Bazzurro P, Castro JM, Crowley H, Dolsek M, Galasso C, Lagomarsino S, Monteiro R, Perrone D, Pitilakis K, Vamvatsikos D (2019) Current Challenges and Future Trends in Analytical Fragility and Vulnerability Modelling. Earthq Spectra. https://doi.org/10.1193/042418EQS101O.042418EQS101O

Silva V, Amo-Oduro D, Calderon A, Costa C, Dabbeek J, Despotaki V, Martins L, Pagani M, Rao A, Simionato M, Viganò D, Yepes-Estrada C, Acevedo A, Crowley H, Horspool N, Jaiswal K, Journeay M, Pittore M (2020) Development of a global seismic risk model. Earthq Spectra 36(1suppl):372–394. https://doi.org/10.1177/8755293019899953

SodM (State Supervision of Mines) (2016) Risk analysis methodology for induced earthquakes due to gas production: Interim guideline to address Article 24.1.p of the Mining Decree, version 1.2. PO Box 24037:2490 AA The Hague

Sousa R, Silva V, Rodrigues H (2022) The importance of indirect losses in the seismic risk assessment of industrial buildings–An application to precast RC buildings in Portugal. Int J Disaster Risk Reduct 74:102949

Stewart J, Afshari K, Hashash Y (2014) Guidelines for performing hazard-consistent one-dimensional ground response analysis for ground motion prediction

Taylor J, Çelebi M, Greer A, Jampole E, Masroor A, Melton S, Norton D, Paul N, Wilson E, Xiao Y (2017) Damages after the M5 Cushing earthquake (Nov 7 2016) in Oklahoma. EERI

Teng G, Baker JW, Wald DJ (2022) Evaluation of Intensity Prediction Equations (IPEs) for Small-Magnitude Earthquakes. Bull Seismol Soc Am 112(1):316–330. https://doi.org/10.1785/0120210150

van der Voort N, Vanclay F (2015) Social impacts of earthquakes caused by gas extraction in the Province of Groningen, The Netherlands. Environ Impact Assess Rev 50:1–15. https://doi.org/10.1016/j.eiar.2014.08.008

van Elk J, Bourne SJ, Oates SJ, Bommer JJ, Pinho R, Crowley H (2019) A Probabilistic Model to Evaluate Options for Mitigating Induced Seismic Risk. Earthq Spectra 35(2):537–564. https://doi.org/10.1193/050918EQS118M

van Ginkel J, Ruigrok E, Stafleu J, Herber R (2022) Development of a seismic site-response zonation map for the Netherlands. Nat Hazards Earth Syst Sci 22(1):41–63. https://doi.org/10.5194/nhess-22-41-2022

van Thienen-Visser K, Roholl JA, van Kempen BMM, Muntendam-Bos AG (2018) Categorizing seismic risk for the onshore gas fields in the Netherlands. Eng Geol 237:198–207. https://doi.org/10.1016/j.enggeo.2018.02.004

Verdon JP, Bommer JJ (2020) Green, yellow, red, or out of the blue? An assessment of Traffic Light Schemes to mitigate the impact of hydraulic fracturing-induced seismicity. J Seismolog. https://doi.org/10.1007/s10950-020-09966-9

Vilarrasa V, De Simone S, Carrera J, Villaseñor A (2021) Unraveling the Causes of the Seismicity Induced by Underground Gas Storage at Castor, Spain. Geophys Res Lett 48(7). https://doi.org/10.1029/2020GL092038

Watkins TJ, Verdon JP, Rodríguez-Pradilla G (2023) The temporal evolution of induced seismicity sequences generated by low-pressure, long-term fluid injection. J Seismolog 27(2):243–259

Weatherill G, Kotha SR, Cotton F (2020) Re-thinking site amplification in regional seismic risk assessment. Earthq Spectra 36(1suppl):274–297. https://doi.org/10.1177/8755293019899956

Weatherill G, Crowley H, Roullé A, Tourlière B, Lemoine A, Gracianne C, Kotha SR, Cotton F (2023) Modelling site response at regional scale for the 2020 European Seismic Risk Model (ESRM20). Bull Earthq Eng 21(2):665–714. https://doi.org/10.1007/s10518-022-01526-5

Wood HO, Neumann F (1931) Modified Mercalli intensity scale of 1931. Bull Seismol Soc Am 21(4):277–283

Yepes-Estrada C, Silva V, Valcárcel J, Acevedo AB, Tarque N, Hube MA, María HS (2017) Modeling the residential building inventory in South America for seismic risk assessment. Earthq spectra 33(1):299–322

Yepes-Estrada C, Calderon A, Costa C, Crowley H, Dabbeek J, Hoyos MC, Silva V (2023) Global building exposure model for earthquake risk assessment. Earthq Spectra 39(4):2212–2235

Zalachoris G, Rathje EM (2019) Ground motion model for small-to-moderate earthquakes in Texas, Oklahoma, and Kansas. Earthq Spectra 35(1):1–20

Zhou W, Lanza F, Grigoratos I, Schultz R, Cousse J, Trutnevyte E, Muntendam-Bos A, Wiemer S (2024) Managing induced seismicity risks from enhanced geothermal systems: A good practice guideline. Rev Geophys. https://doi.org/10.1029/2024RG000849